CrossMark

Effects of Disodium Phosphate Concentration (Na$_2$HPO$_4$·2H$_2$O) on Microstructure and Corrosion Resistance of Plasma Electrolytic Oxidation (PEO) Coatings on 2024 Al Alloy

Arash Fattah-alhosseini, Seyed Omid Gashti, and Maryam Molaie

Since the electrolyte composition plays a pivotal role in the microstructure and corrosion behavior of plasma electrolytic oxidation (PEO) coatings, the effects of disodium phosphate (Na$_2$HPO$_4$·2H$_2$O) concentration on the microstructure and corrosion resistance of PEO coatings fabricated on 2024 Al alloy were studied in this investigation. Accordingly, electrolyte with four different concentrations of phosphate ion (5, 10, 15 and 20 g/L) was used. All PEO processes were conducted at constant current density of 15 A/dm^2 for 15 min. The surface and cross-sectional morphologies of the coatings indicated that the coating formed in the electrolyte with 10 g/L Na$_2$HPO$_4$·2H$_2$O (with 9.14 μm thickness) had the most compact and uniform structure with the lowest and smallest micropores. Furthermore, studying the corrosion behavior of samples in 3.5 wt.% NaCl solutions by electrochemical impedance spectroscopy (EIS) and potentiodynamic polarization tests revealed that the sample coated in the electrolyte with 10 g/L Na$_2$HPO$_4$·2H$_2$O had the highest corrosion potential, the lowest corrosion current density and, accordingly, the best corrosion resistance. The corrosion resistance of this coating was $4.574 \times 10^5 \, \Omega \, cm^2$, which could increase the corrosion resistance of uncoated 2024 Al alloy substrate 48 times. The x-ray diffraction pattern of this coating proved that the coating was composed of α-Al$_2$O$_3$ and γ-Al$_2$O$_3$ phases.

1. Introduction

Due to the significant properties such as high strength-to-weight ratio, low density, high thermal and electrical conductivities, ease of fabrication and recycling potential, Al and its alloys are widely used in many industries such as aerospace, automobile, textile, construction and high-speed trains. However, qualities including low surface hardness, relatively low wear and corrosion resistance and high friction coefficient have restricted their applications (Ref 1-4). Therefore, these reactive alloys and other light metals need careful finishing operation in order to produce surface layers with high wear and corrosion resistance (Ref 5). Alumina (Al$_2$O$_3$) is an advanced ceramic material that can improve resistance to wear, corrosion, oxidation and high-temperature attack when coated on the metal materials, including Al and its alloys (Ref 6). There are many coating techniques for metallic materials, such as hydrothermal, vapor deposition, sol–gel, thermal oxidation and anodic oxidation (Ref 7). Because of high energy consumption and high temperature of the aforementioned methods, they are not

appropriate for materials with low melting point (e.g., Al). In this regard, plasma electrolytic oxidation (PEO), also called micro-arc oxidation (MAO), as a relatively new method was discovered (Ref 8, 9). The PEO process, derived from conventional anodizing, can produce hard and thick ceramic coatings on light metals such as Al, Mg and Ti and their alloys by plasma discharges in an aqueous solution under high voltage with low energy consumption (Ref 3, 8, 10). Coatings produced through this procedure have high micro-hardness, good adhesion to the substrate, high insulation resistance, good wear and corrosion resistance, high-temperature shock and electronic insulation (Ref 11). Generation of many short-lived and fine microdischarges on the substrate surface due to the instantaneous and local dielectric breakdown of the growing coating under high electric field controls the coating formation mechanism (Ref 2, 12, 13). Many parameters such as electrolyte composition, electrolyte temperature, oxidation time, substrate chemical composition, current density, current mode, applied voltage, frequency and duty cycle can influence the properties of the PEO coatings (Ref 14, 15). Among these factors, the electrolyte composition owing to the participation of electrolyte substances in the coating formation reactions during the PEO process is the most important parameter. Structure, composition and other properties of the PEO coating alter with changing the electrolyte composition (Ref 16). Tseng et al. (Ref 17) have confirmed that changing the concentration of Na$_2$WO$_4$ in the electrolyte greatly affected the morphologies, phase compositions, micro-hardness and corrosion resistances of the PEO coatings. They showed that increasing the Na$_2$WO$_4$ concentration in the electrolyte increased the coating thickness, the amount of α-Al$_2$O$_3$ phase, micro-hardness and corrosion resistance and decreased the friction coefficient. Wang et al. Ref 18 have found that adding

Arash Fattah-alhosseini, Seyed Omid Gashti, and **Maryam Molaie**, Department of Materials Engineering, Bu-Ali Sina University, Hamedan 65178-38695, Iran. Contact e-mail: m.molaie93@yahoo.com.

NaF to aluminate-based electrolyte could decrease the surface roughness, increase the thickness of the inner compact layer and also improve the corrosion resistance and tribological properties of the PEO coating.

In the current study, different PEO coatings were fabricated on 2024 Al alloy substrate in phosphate-based electrolyte with four different concentrations of disodium phosphate ($Na_2HPO_4 \cdot 2H_2O$). Then, the effects of $Na_2HPO_4 \cdot 2H_2O$ concentration on the microstructure and corrosion behavior of PEO coatings were investigated.

2. Experimental

2024 Al alloy specimens with the dimensions of 20 mm × 20 mm × 1 mm were used as the substrate material for the PEO processes. Prior to PEO process, all samples were annealed at 420 °C temperature for 3 h. After that, they were polished with #400 to #2000 grit SiC abrasive papers, washed with distilled water and dried with cold air. The phosphate-based electrolytes made of 4 g/L $Na_2SiO_3 \cdot 5H_2O$, 1 g/L KOH and four different concentrations of $Na_2HPO_4 \cdot 2H_2O$, as given in Table 1, were used for coating processes. The PEO processes lasted 15 min, under a constant current density of 15 A/dm^2 by PM700/7 PRC (IPS) with DC power supply. During the experiment, the temperature of the electrolyte was cooled below 35 °C using a cooling system. After each treatment, the coated sample was rinsed with distilled water and dried in cold air. The 2024 Al alloy sample and a stainless steel container were used as anode and cathode, respectively. The values of conductivity and pH of different electrolyte solutions were measured by PTR7 and Lf91 instruments, respectively. The surface and cross-sectional morphologies of the coatings were investigated by JEOL JSM-840A scanning electron microscope (SEM). The average micropore size and thickness of the coatings were measured by Digimizer software. The phase composition of the coating was studied by x-ray diffraction using an APD 2000 diffractometer with a Cu Kα radiation by scanning in the $2\theta = 20°\text{-}90°$ range. Also, the elemental analysis of the coated sample was analyzed using a Link AN 10/55 S energy-dispersive x-ray spectrometer (EDS). Corrosion behavior of the uncoated and coated samples was studied with electrochemical impedance spectroscopy (EIS) and potentiodynamic polarization tests in 3.5 wt.% NaCl solutions at room temperature by the μAutolab Type III/FRA2 system. In these tests, a three-electrode flat cell, including platinum plate as the counter electrode and Ag/AgCl saturated in KCl as the reference electrode, was used. Similarly, a sample with an exposed area of 0.4 cm^2 was utilized as the working electrode. All the measurements related to the corrosion behavior were carried out with the NOVA 1.11 impedance software. All the uncoated and coated samples were immersed in 3.5 wt.% solutions for 2 h to reach a stable open-circuit potential. EIS tests were employed in the frequency range of 10 mHz to 100 kHz with the amplitude of 10 mV. Then by applying − 250 mV potential, compared to the open-circuit potential, potentiodynamic polarization test was conducted at a scan rate of 1 mV/s on the specimens.

3. Results and Discussion

3.1 Voltage–Time Behavior

As constant current mode was used in all processes, voltage–time responses of the coated samples in electrolytes with different concentrations of $Na_2HPO_4 \cdot 2H_2O$ are shown in Fig. 1. As can be seen, changing the electrolyte composition has affected the voltage–time behavior of the samples during the PEO processes. All voltage–time curves for four different samples depicted three stages. At the beginning of the PEO process, stage 1, due to the formation of a very thin insulating barrier oxide film on the surface of 2024 Al alloy substrate (anode), voltage increased linearly and quickly by the passage of time (about 1 min). In stage 2, the voltage increased with time at a lower ratio compared with stage 1, and then, the breakdown of weak parts of the oxide film occurred. After exceeding the breakdown voltage, many small white transient sparks, which were essentially specified by the composition and concentration of the electrolyte and base metal nature (Ref 19), were emerged on the substrate surface and the voltage slowly increased just some 3 min after the onset of the processing cycle. In this level, the growth rate of the coating decreased because of the coating growth and dissolution coincidence (Ref 20-22). In stage 3, known as the micro-arc stage, voltage reached a relatively stable value and sparks became more intense. Also, the color of sparks changed to yellow and then gradually turned orange (Ref 20, 21). Changing the concentration of $Na_2HPO_4 \cdot 2H_2O$ in the electrolyte led to changing the values of electrolyte conductivity and breakdown voltage. The variation of the conductivity with respect to the breakdown
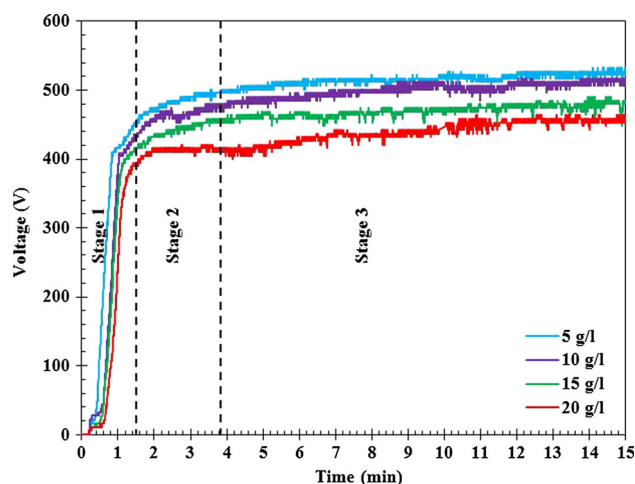
Table 1 Electrolyte compositions for different PEO processes

$Na_2HPO_4 \cdot 2H_2O$, g/L	$Na_2SiO_3 \cdot 5H_2O$, g/L	KOH, g/L	pH
5	4	1	12.20
10	4	1	11.83
15	4	1	11.52
20	4	1	11.33

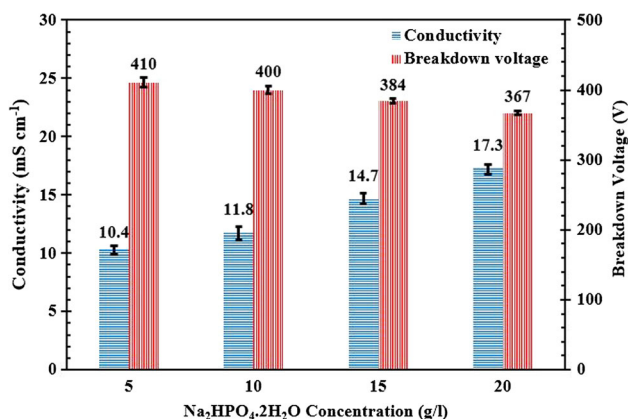**Fig. 1** Voltage–time curves of PEO treated 2024 Al alloy samples

Fig. 2 Variation of the conductivity with respect to the breakdown voltage for different PEO electrolytes

voltage for different electrolytes is depicted in Fig. 2. The relation between the electrolyte conductivity (K) and the breakdown voltage (V_b) is shown in Eq (1). In this equation, a_B and b_B are constant values related to the metal and electrolyte composition. Therefore, increasing the electrolyte conductivity requires lower arcing energy, thereby decreasing the breakdown voltage of the oxide film (Ref 23). This may be due to the fact that the anionic species of the electrolyte were absorbed in the oxide film with an increased rate. Hence, the primary electrons just injected to the conduction band of the oxide found greater density (Ref 24).

$$V_b = a_B + b_B \log\left(\frac{1}{K}\right) \qquad (Eq\ 1)$$

Therefore, increasing the concentration of $Na_2HPO_4\cdot2H_2O$ (5-20 g/L) in the electrolyte, due to the increase in the electrolyte conductivity, led to the reduction in the voltage needed for breaking down the resistance of the dielectric layer. On the other hand, to reach the breakdown voltage, the ease of the dielectric barrier layer formation and the plasma discharge occurrence were in a direct relationship with the time duration (Ref 20, 25). Thus, increasing the concentration of $Na_2HPO_4\cdot2H_2O$ (5-20 g/L) led to increasing the time for the breakdown voltage and the formation of barrier film, and shortening the required duration for the spark discharges to appear. On the other hand, at first, because of reducing the breakdown voltage, increasing the concentration of $Na_2HPO_4\cdot2H_2O$ from 5 to 10 g/L led to the reduction in the size and intensity of the sparks. However, adding the concentration of $Na_2HPO_4\cdot2H_2O$ (up to 20 g/L), due to the greater conductivity, caused more intense and larger sparks.

3.2 Coatings Microstructure

3.2.1 Surface Morphology of the Coatings. The surface morphologies and average size of micropores of different PEO coatings fabricated on the surface of 2024 Al alloy substrate are shown in Fig. 3 and 4, respectively. It is obvious that changing the concentration of $Na_2HPO_4\cdot2H_2O$ in the electrolyte has influenced the surface morphologies of the PEO coatings. All four coatings due to the nature of PEO process exhibited the porous structure with crater shape micropores. During the PEO process, as the micro-arcs and the following discharges occur,

gas evolution channels are created because of the rapid melting and solidification impact on the substrate surface (Ref 18, 25). The breakdown voltage, and evolution and characteristics of the discharging sparks during the PEO process, intimately correlated with the conductivity of the electrolyte, influence the formation of porous structure and change the surface morphology and thickness of the coatings. The larger the sparks, the bigger the micropore form on the surface of the coating, whereas the shorter the sparks, the lesser the amount and size of the micropore shape (Ref 26). Higher breakdown voltage leads to higher level of discharge energy and forms larger micropores with non-uniform dispersion on the surface of the coating (Ref 27). Here, at first, increasing the concentration of $Na_2HPO_4\cdot2H_2O$ (from 5 to 10 g/L) in the electrolyte, due to an increase in the conductivity, a decrease in the breakdown voltage and the size and the intensity of sparks, led to an increment in the compactness and uniformity of the structure and the reduction in the micropore size and number. Then by adding to the concentration (from 10 to 20 g/L), the size and number of the micropores are increased. This phenomenon was related to the increase in the size and intensity of spark discharges because of the enhanced electrolyte conductivity (Ref 28). The coated sample in the electrolyte containing 5 g/L $Na_2HPO_4\cdot2H_2O$ showed the most non-uniform structure with large solidified oxide particles and the largest average micropore size in comparison with three other coatings. Low conductivity of the electrolyte, leading to the greater sparks in the coating process, and higher final and breakdown voltage might result in this phenomenon. Consequently, the coated sample in the electrolyte with 10 g/L $Na_2HPO_4\cdot2H_2O$ had the most uniform and compact structure with the lowest and smallest micropores (with average size of 1.44 μm).

3.2.2 Thickness of Coatings. Figure 5 and 6 show the cross-sectional morphologies and thickness values of different PEO coatings, respectively. As can be concluded, the thickness of the coatings increased (from 8.07 to 12.04 μm) by increasing the concentration of $Na_2HPO_4\cdot2H_2O$ (5-20 g/L) in the electrolyte. Indeed, rising the PO_4^{3-} ion concentration in the electrolyte involved more components from the applied solution to be incorporated into the coating, thereby increasing the coating growth rate and thickness through poly-reactions and deposition on the surface (Ref 29, 30). On the other hand, the increased concentration of $Na_2HPO_4\cdot2H_2O$ in the electrolyte led to an increment in the electrolyte conductivity and as a result, the rate of the film formation dominated the rate of anodic dissolution forming the thicker coating (Ref 23). All four coatings were compact without any obvious deep porosity, but the fabricated coating using the electrolyte containing 5 g/L $Na_2HPO_4\cdot2H_2O$ was less uniform in comparison with the others. Also, for all of the specimens, the interface of the substrate and coating was continuously observed, demonstrating acceptable coating adhesion to the substrate.

3.3 Corrosion Behavior

3.3.1 Electrochemical Impedance Spectroscopy (EIS). The Nyquist plots derived from EIS data are shown in Fig. 7. In these plots, the real part of the impedance was plotted versus its imaginary part at each frequency after 2-h immersion in 3.5 wt.% NaCl solution. As can be seen, in all frequency regions, the uncoated 2024 Al alloy substrate had one capacitive semicircle. The oxide layer made on the surface of
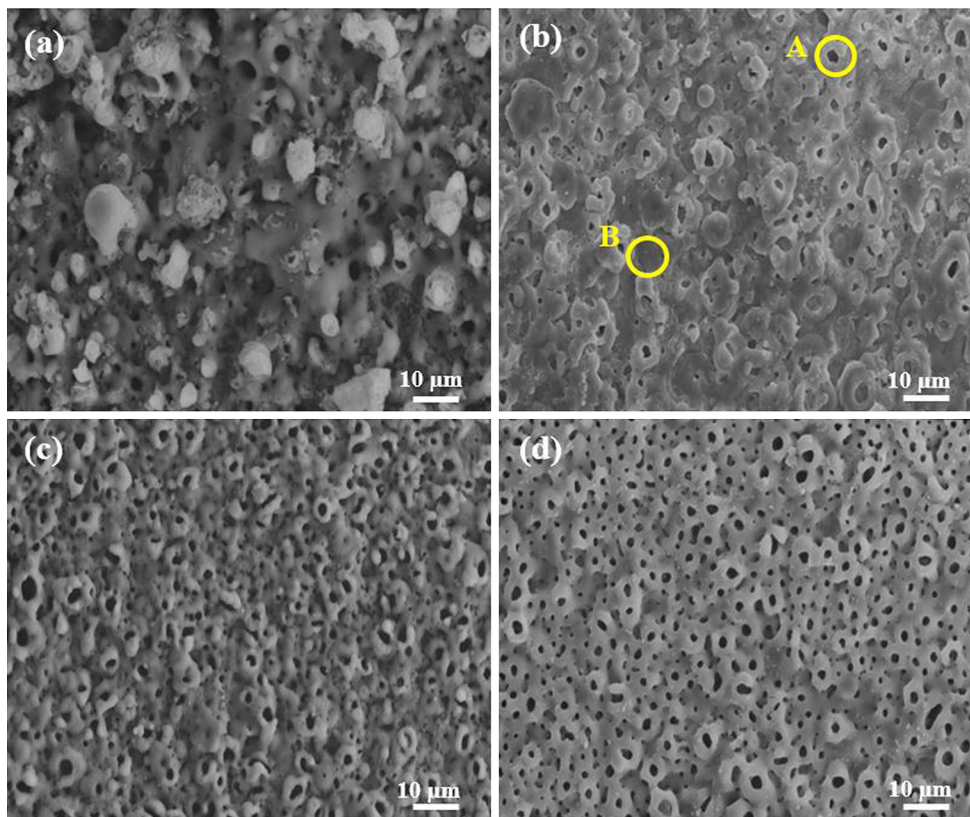
Fig. 3 Surface morphologies of the PEO coatings formed in electrolytes with different concentrations of $Na_2HPO_4 \cdot 2H_2O$ at the magnification of $\times 1000$: (a) 5 g/L; (b) 10 g/L; (c) 15 g/L; (d) 20 g/L
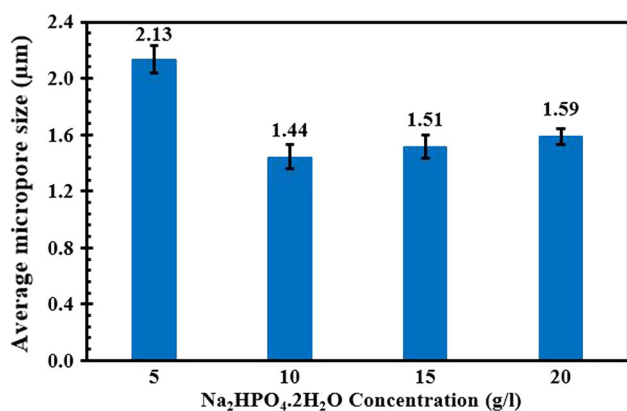

Fig. 4 Average micropore size of different PEO coatings

the substrate might cause this quality; therefore, in the electrical equivalent circuit, there would be just one single time constant presented in Fig. 8(a). The corrosion resistance of uncoated 2024 Al alloy was obtained by measuring the diameter of the semicircle in the Nyquist plot. Conversely, the Nyquist plots of all coated samples included two capacitive semicircles in electrolytes having varying degrees of concentration of $NaH_2PO_4 \cdot 2H_2O$. The smaller semicircle appeared at high frequencies was related to the porous outer layer, and the bigger semicircle appeared at low frequencies was referred to as the compact inner layer (Ref 29). The electrical equivalent circuits that were used to simulate the impedance data of the

uncoated 2024 Al alloy and the coated samples are illustrated in Fig. 8. The electrical equivalent circuit in Fig. 8(a) was suggested for the bare 2024 Al alloy. In this circuit, R_s ($3.1 \, \Omega \, cm^2$), R_I and Q_I were the solution resistance, corrosion resistance and constant phase element, respectively. In order to fit the impedance plots of the coated samples, the electrical equivalent circuit given in Fig. 8(b) was used. In this circuit, R_I and Q_I were related to the corrosion resistance and the constant phase element of the compact inner layer, and R_O and Q_O are referred to as the porous outer one. Also, R_S was the solution resistance ($2.8 \pm 1 \, \Omega \, cm^2$). Two factors mainly determine the value of R_s, namely the electrochemical cell geometry and the corrosion test solution conductivity (Ref 29). The extracted corrosion resistance values of the inner and outer layers from the electrical equivalent circuit of all samples are listed in Fig. 9. The corrosion resistance of 2024 Al alloy substrate was very low ($9.4 \times 10^3 \, \Omega \, cm^2$). Accordingly, in order to improve its corrosion resistance, it was necessary to apply a coating on its surface. As is clear, because of the higher values of corrosion resistance of inner layers compared with those of the outer layer, the corrosion resistance of the PEO coatings was attributed to the corrosion resistance of the inner layer, and the outer layer did not effectively improve the corrosion resistance of the uncoated 2024 Al alloy substrate. All coatings exhibited better corrosion resistance compared to the uncoated 2024 Al alloy substrate. This meant that the PEO technique was an effective coating process improving the corrosion resistance of 2024 Al alloy substrate. Indeed, the coatings did not allow the corrosive species to be in contact with the surface of the metal,
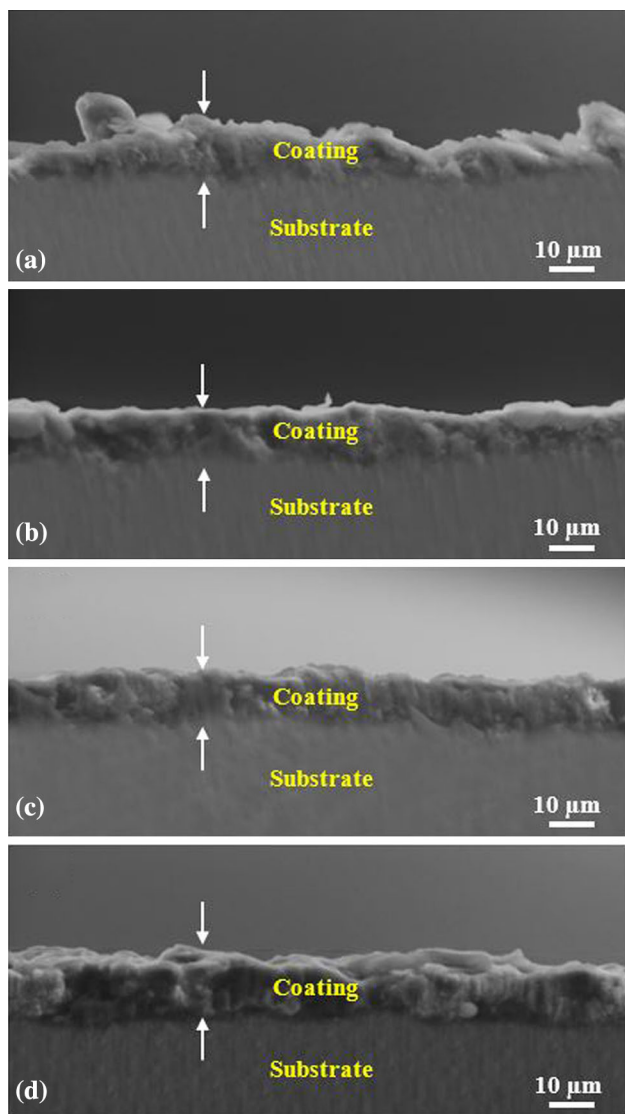
Fig. 5 Cross-sectional morphologies of the PEO coatings formed in electrolytes with different concentrations of $Na_2HPO_4 \cdot 2H_2O$ at the magnification of $\times 1000$: (a) 5 g/L; (b) 10 g/L; (c) 15 g/L; (d) 20 g/L

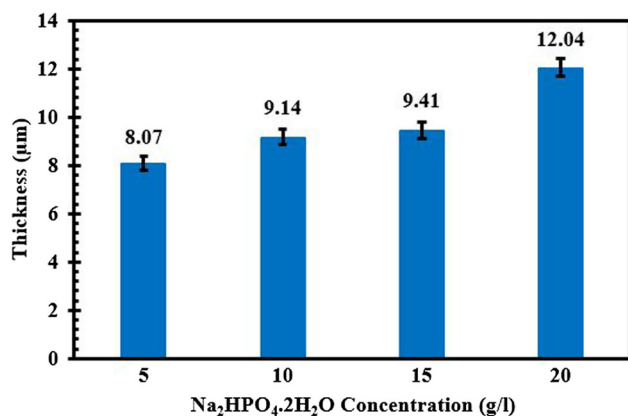**Fig. 6** Thickness of different PEO coatings

thereby impeding the corrosion. At first, increasing the concentration of $Na_2HPO_4 \cdot 2H_2O$ (5-10 g/L) in the electrolyte led to a remarkable increase in the corrosion resistance of both inner and outer layers, and with increasing the concentration more (up to 20 g/L), the corrosion resistance reduced. Therefore, the coated sample in the electrolyte with 10 g/L $Na_2HPO_4 \cdot 2H_2O$ showed the best corrosion resistance among all other samples. The corrosion resistance of this sample was $4.574 \times 10^5 \ \Omega \ cm^2$, which was 48 times greater than that of the uncoated 2024 Al alloy substrate. Also, the sample coated in the electrolyte with 5 g/L $Na_2HPO_4 \cdot 2H_2O$ had the minimum corrosion resistance ($1.69 \times 10^4 \ \Omega \ cm^2$) in comparison with the concentrations of 15 and 20 g/L.

3.3.2 Potentiodynamic Polarization. The PEO process has an influence on corrosion from three main aspects as follows: (1) "retarding" effect, decelerating corrosive species ingress in the corrosion process; (2) "blocking" effect, limiting the substrate contact area with the surrounding solution; and (3) "passivation" effect, concealing defective/active substrate (Ref 31). The potentiodynamic polarization plots for uncoated 2024 Al alloy substrate and coated samples in 3.5 wt.% NaCl solutions at room temperature are shown in Fig. 10. The corrosion potential (E_{corr}) and corrosion current density (i_{corr}) values extracted from the potentiodynamic polarization plots are given in Fig. 11. While i_{corr} shows the sample corrosion rate, E_{corr} represents the thermodynamic tendency for corrosion (Ref 32). Though the corrosion potential (E_{corr}) and the corrosion current density (i_{corr}) are often considered to evaluate the specimens corrosion behavior, the corrosion current density has taken precedence over the corrosion potential (E_{corr}) and is mainly used to determine the corrosion resistance. The lower corrosion current density indicates the higher corrosion resistance (Ref 33). Therefore, all coated samples, due to their lower corrosion current density, had higher corrosion resistance compared to the bare substrate. However, the corrosion potential of the coated sample in the electrolyte containing 5 g/L $Na_2HPO_4 \cdot 2H_2O$ was more negative than that of the substrate. In fact, the exchange of electrical charges and the transference of the electrons on the surface of the samples are both decreased by the low electrical conductivity of Al_2O_3 coatings, necessary for electrochemical corrosion (Ref 34). In the current study, the thickness and porosity were the two vital elements in controlling the corrosion behavior of the coatings as the concentration of $Na_2HPO_4 \cdot 2H_2O$ was the only investigated variable. Pitting corrosion is the main defect observed in alumina coatings in the NaCl solution. It could be concluded that considerable defects within the outer layer resulting from rapid melting and solidification during the discharge occurrence during the PEO process in the electrolyte are suitable paths for the aggressive Cl^- anions penetration causing corrosion. Accordingly, the fabrication of thicker coatings with denser and finer microstructures containing smaller pores can effectively enhance the corrosion resistance through the inhibition of Cl^- attack in the NaCl solution (Ref 35-37). Consequently, increasing the concentration of $Na_2HPO_4 \cdot 2H_2O$ in the electrolyte (5-10 g/L) enhanced the coating uniformity and compactness, reduced the number and size of micropores, increased the coating thickness and, subsequently, improved the corrosion resistance. However, higher concentration of $Na_2HPO_4 \cdot 2H_2O$ (up to 20 g/L), by increasing the coating thickness, would lead to a reduction in the corrosion resistance of the coating as the
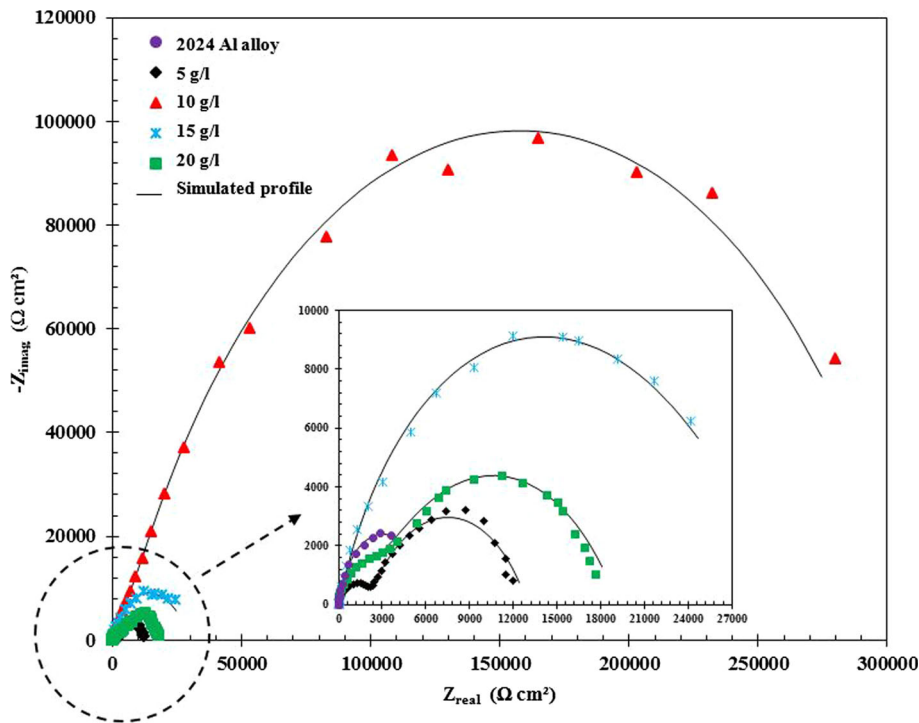
Fig. 7 Nyquist plots for 2024 Al alloy substrate and different coated samples after 2-h immersion in 3.5 wt.% NaCl solutions
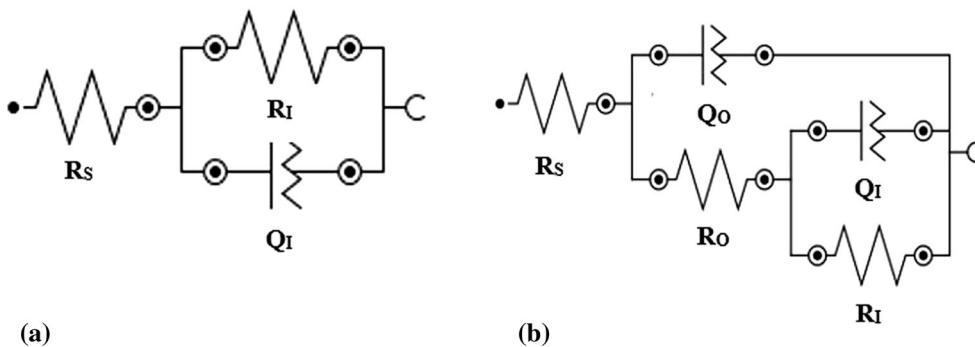

Fig. 8 EIS equivalent circuit of (a) 2024 Al alloy substrate and (b) PEO coating

size and number of micropores would increase. Based on what has so far explained, no defects must be found in the coating including micro-cracks and porosities if we want to achieve higher corrosion properties (Ref 38). Therefore, the coated sample in the electrolyte with 10 g/L $Na_2HPO_4 \cdot 2H_2O$ had the noblest corrosion potential ($-$ 0.603 V) and the lowest corrosion current density (8.7×10^{-8} A/cm^2) and, accordingly, displayed the best corrosion resistance. In this sample, the corrosion current density was about two orders lower than that of the uncoated 2024 Al alloy substrate. Indeed, the uniform compact coating of this study containing few cracks or porosities led to the great corrosion behavior of the sample,

decreasing the dispersion of the destructive Cl$^-$ anions to the Al substrate.

3.4 Coating Phase Composition

Figure 12 displays the EDS analysis of two selected regions (shown in Fig. 3b) of the coated sample in the electrolyte with 10 g/L $Na_2HPO_4 \cdot 2H_2O$ (the optimum concentration). Points A and B were related to the micropore and the surface of coating, respectively. Both EDS of the coating surface and micropore showed the peaks of Al relating to the 2024 Al alloy substrate, and O, Si and P elements coming from the electrolyte
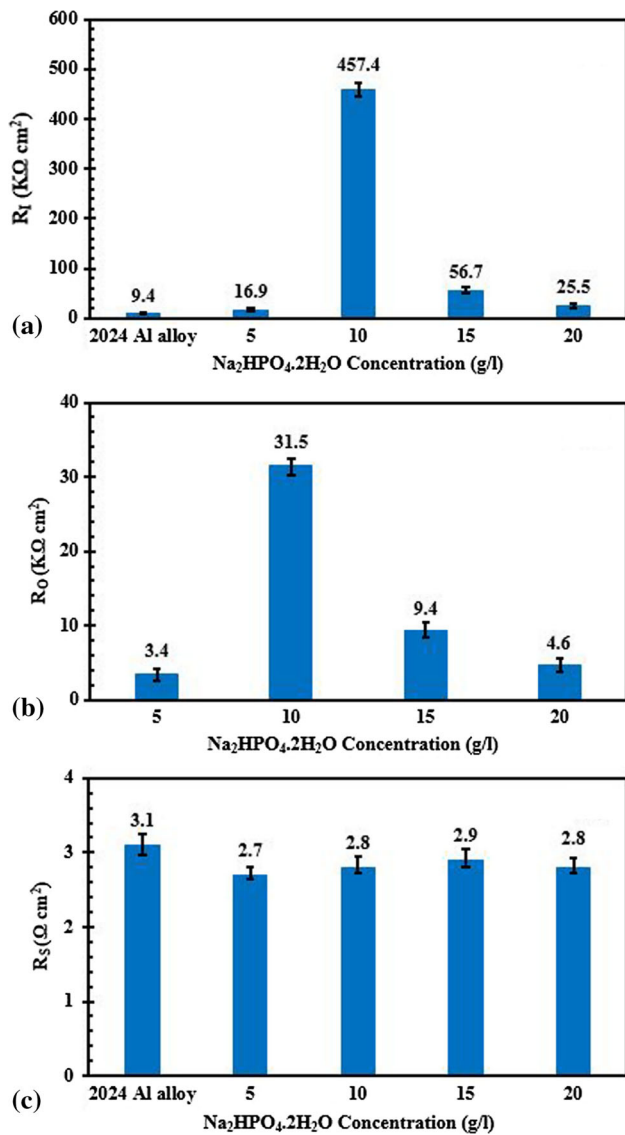
Fig. 9 Extracted data of the Nyquist plots for 2024 Al alloy substrate and different coated samples: (a) corrosion resistance of inner layer; (b) corrosion resistance of outer layer; (c) solution resistance
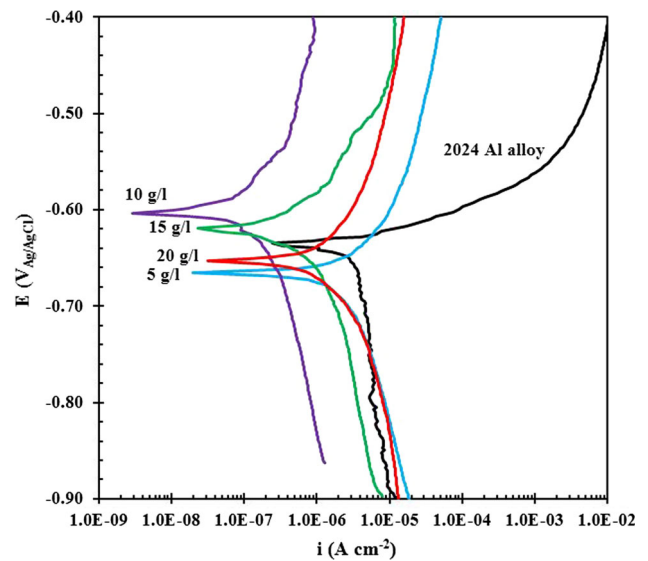

Fig. 10 Potentiodynamic polarization curves of 2024 Al alloy substrate and different coated samples in 3.5 wt.% NaCl solutions
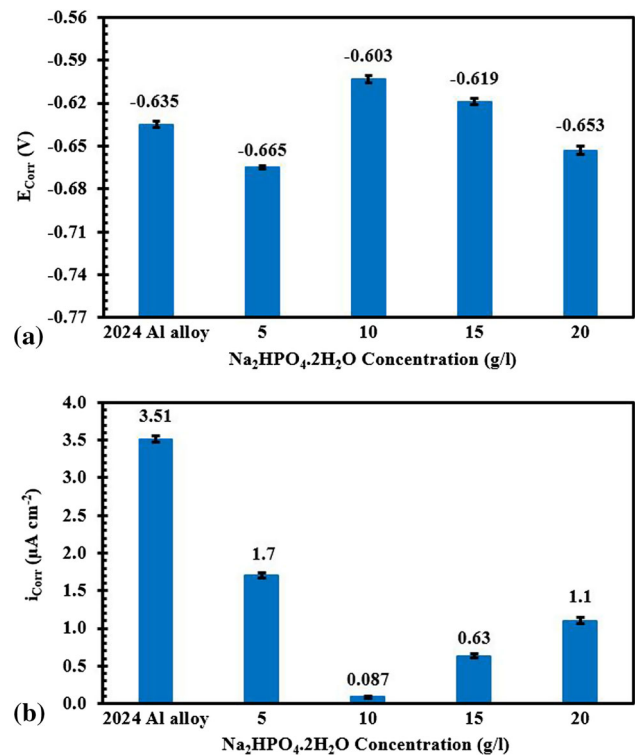
Fig. 11 Analysis of data of potentiodynamic polarization curves for 2024 Al alloy substrate and different coated samples: (a) corrosion potential; (b) corrosion current density

components ($Na_2HPO_4\cdot2H_2O$ and $Na_2SiO_3\cdot5H_2O$). While the intensity of Al peak in the EDS of the region A (micropore) was more than that in the region B (surface), the Si and P peaks were more intense in the EDS of region B. This was due to the Al egress from where sparks produced and the electrochemical participation of Si and P in the reactions was assisted by micro-sparks resulting in their adsorption to the coating. In other words, conventionally, heat-affected zones and micro-arc discharging zones are both created throughout PEO treatment. These two zones are considered as the adsorption centers due to their high energy resulting from the super-high temperature. This causes the solute anions to be adsorbed in the surface of the coating (Ref 39). In order to evaluate the phase composition of the coating and to complete the EDS analysis, the XRD pattern of this sample is shown in Fig. 13. As can be seen, the coating was composed of α-Al_2O_3 and γ-Al_2O_3 phases, generally the main phases of the PEO coatings on Al and its alloys (Ref 40). The α-Al_2O_3 is a thermodynamically

stable phase at all temperatures with a high melting point of 2050 °C and the hexagonal dense close-packed structure providing the highest stability. But the γ-Al_2O_3 is a metastable phase with face-centered cubic structure, which can be easily transformed to the α-Al_2O_3 at temperatures over 1000 °C (Ref 41-43). The following processes are commonly

Fig. 12 EDS spectra of the coated sample in the electrolyte with 10 g/L Na$_2$HPO$_4$·2H$_2$O: (a) region A; (b) region B

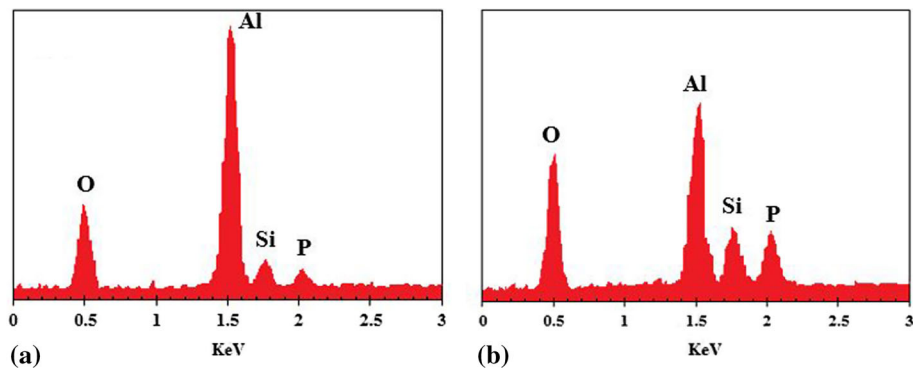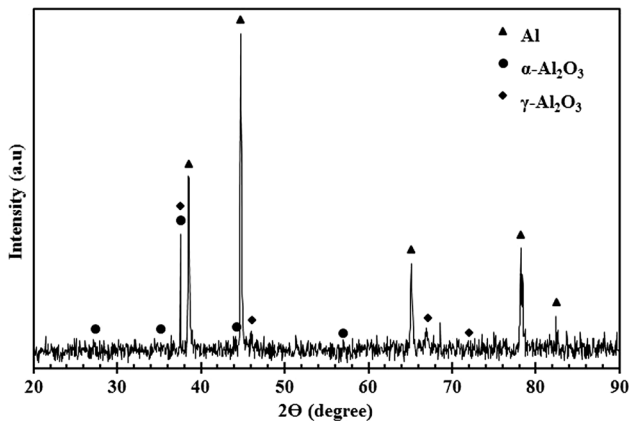**Fig. 13** XRD pattern of the coated sample in the electrolyte with 10 g/L Na$_2$HPO$_4$·2H$_2$O

suggested for the in situ growth of the Al$_2$O$_3$ film formed on the aluminum alloy using MAO technique.

Cathode reaction:

$$2H^+ + 2e \rightarrow H_2 \uparrow \qquad \text{(Eq 2)}$$

Anode reaction:

$$HPO_4^{2-} + H_2O \rightarrow OH^- + H_2PO_4^- \qquad \text{(Eq 3)}$$

$$4OH^- \rightarrow 2H_2O + O_2 \uparrow + 4e \qquad \text{(Eq 4)}$$

$$Al \rightarrow Al^{3+} + 3e \qquad \text{(Eq 5)}$$

$$Al^{3+} + 3OH^- \rightarrow Al(OH)_3 \qquad \text{(Eq 6)}$$

$$2Al(OH)_3 \rightarrow Al_2O_3 + 3H_2O \qquad \text{(Eq 7)}$$

$$2Al^{3+} + 3SiO_3 \rightarrow 3SiO_2 + Al_2O_3 \qquad \text{(Eq 8)}$$

$$2Al^{3+} + 3O^{2-} \rightarrow Al_2O_3 \qquad \text{(Eq 9)}$$
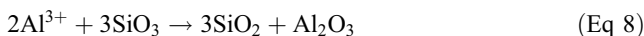
Al^{3+} from the substrate reacts with OH$^-$ and O^{2-} in the electrolyte, and molten Al$_2$O$_3$ is consequently formed because of the higher voltage and temperature initiated by discharge sparks. Instantaneously, the molten Al$_2$O$_3$ throws out of the discharge channels and makes the ceramic coatings by suppressing the electrolyte with a high cooling rate (Ref 44). Furthermore, no trace of phosphorus-based crystalline phases was found in the XRD pattern in spite of the phosphate existence in the electrolyte. Also, because of the low thickness of the coating and the existence of porosity on its surface, x-ray could easily penetrate through the surface and as a result, diffraction peaks of Al substrate were detected in the XRD pattern.

4. Conclusion

In this study, the effects of disodium phosphate (Na$_2$HPO$_4$·2H$_2$O) concentration on the microstructure and corrosion resistance of the alumina (Al$_2$O$_3$) PEO coatings on the surface of 2024 Al alloy were investigated. The obtained results are as follows:

1. The increase in the concentration of Na$_2$HPO$_4$·2H$_2$O (5-20 g/L) in the electrolyte caused a decrease in the breakdown voltage and an increase in the conductivity, and as a result affected the coating morphology. Surface and cross-sectional morphologies of the coatings indicated that increasing the concentration of Na$_2$HPO$_4$·2H$_2$O (5-10 g/L) in the electrolyte increased the compactness and uniformity of the structure and decreased the average size and the number of micropores. However, higher concentrations (10 to 20 g/L), despite increasing the thickness, resulted in the deterioration of the microstructure by increasing the average size and the number of micropores. Therefore, the coated sample in the electrolyte with 10 g/L Na$_2$HPO$_4$·2H$_2$O (with 9.14 μm thickness) had the most uniform and compact structure with the lowest and smallest micropores (with the average size of 1.43 μm).

2. EIS tests of the uncoated 2024 Al alloy substrate and coated samples indicated that increasing the concentration of Na$_2$HPO$_4$·2H$_2$O in the electrolyte (5-10 g/L) led to the improvement of corrosion resistance, and greater concentrations (10-20 g/L) reduced the corrosion resistance. Therefore, the coated sample in the electrolyte with 10 g/L Na$_2$HPO$_4$·2H$_2$O presented the most corrosion resistance ($4.574 \times 10^5 \ \Omega \ cm^2$). The corrosion resistance of this coating was 48 times greater than that of the uncoated 2024 Al alloy substrate. The results of the potentiodynamic polarization measurements exhibited that increasing the concentration of Na$_2$HPO$_4$·2H$_2$O (5-10 g/L) in the electrolyte, due to an increase in the compactness and uniformity and a decrease in the porosity, enhanced the corrosion potential and reduced the corrosion current density of

the coating. In addition, with more increased concentrations (up to 20 g/L), despite the formation of a thicker coating, the corrosion potential was dropped to more negative values and the corrosion current density of the coatings increased because of the porosity increment. Thus, the sample coated in the electrolyte with 10 g/L Na$_2$HPO$_4$·2H$_2$O had the noblest corrosion potential ($-$ 0.603 V) and the lowest corrosion current density (8.7×10^{-8} A/cm^2) and as a result, better corrosion resistance among all samples. The corrosion current density of this coating was about two orders lower in comparison with the uncoated 2024 Al alloy substrate.

3. The EDS analysis of the two regions (surface and micropore) of the coated sample in the electrolyte with 10 g/L Na$_2$HPO$_4$·2H$_2$O (optimum concentration) proved that both regions had Al, O, Si and P elements. The intensity of Al peak was higher and the intensity of Si and P elements peaks was lower in the micropore EDS compared to the coating surface. Also, the XRD pattern of this sample revealed that the coating was composed of α-Al$_2$O$_3$ and γ-Al$_2$O$_3$ phases.

References

1. J.H. Wang, M.H. Du, F.Zh. Han, and J. Yang, Effects of the Ratio of Anodic and Cathodic Currents on the Characteristics of Micro-arc Oxidation Ceramic Coatings on Al Alloys, *Appl. Surf. Sci.*, 2014, **292**, p 658–664

2. V. Dehnavi, B.L. Luan, D.W. Shoesmith, X.Y. Liu, and S. Rohani, Effect of Duty Cycle and Applied Current Frequency on Plasma Electrolytic Oxidation (PEO) Coating Growth Behavior, *Surf. Coat. Technol.*, 2013, **226**, p 100–107

3. V. Shoaei-Rad, M.R. Bayati, H.R. Zargar, J. Javadpour, and F. Golestani-Fard, In Situ Growth of ZrO$_2$-Al$_2$O$_3$ Nano-crystalline Ceramic Coatings Via Micro Arc Oxidation of Aluminum Substrates, *Mater. Res. Bull.*, 2012, **47**, p 1494–1499

4. M. Vakili-Azghandi and A. Fattah-alhosseini, Effects of Duty Cycle, Current Frequency, and Current Density on Corrosion Behavior of the Plasma Electrolytic Oxidation Coatings on 6061 Al Alloy in Artificial Seawater, *Metall. Mater. Trans. A*, 2017, **48**, p 4681–4692

5. F.C. Walsh, C.T.J. Low, R.J.K. Wood, K.T. Stevens, J. Archer, A.R. Poeton, and A. Ryder, Plasma Electrolytic Oxidation (PEO) for Production of Anodised Coatings on Lightweight Metal (Al, Mg, Ti) Alloys, *Trans. IMF*, 2009, **87**, p 122–130

6. X. Shen, X. Nie, H. Hu, and J. Tjong, Effects of Coating Thickness on Thermal Conductivities of Alumina Coatings and Alumina/Aluminum Hybrid Materials Prepared Using Plasma Electrolytic Oxidation, *Surf. Coat. Technol.*, 2012, **207**, p 96–101

7. Ch.H Hsu, H.P. Teng, and F.H. Lu, Effects of Addition of Al (NO$_3$)$_3$ to Electrolytes on Alumina Coatings by Plasma Electrolytic Oxidation, *Surf. Coat. Technol.*, 2011, **205**, p 3677–3682

8. K. Wang, B.H. Koo, Ch.G. Lee, Y.J. Kim, S.H. Lee, and E. Byon, Effects of Electrolytes Variation on Formation of Oxide Layers of 6061 Al Alloys by Plasma Electrolytic Oxidation, *Trans. Nonferrous Met. Soc. China*, 2009, **19**, p 866–870

9. M. Vakili-Azghandi, A. Fattah-alhosseini, and M.K. Keshavarz, Effects of Al$_2$O$_3$ Nano-particles on Corrosion Performance of Plasma Electrolytic Oxidation Coatings Formed on 6061 Aluminum Alloy, *J. Mater. Eng. Perform.*, 2016, **25**, p 5302–5313

10. M. Sabaghi Joni and A. Fattah-alhosseini, Effect of KOH Concentration on the Electrochemical Behavior of Coatings Formed by Pulsed DC Micro-arc Oxidation (MAO) on AZ31B Mg Alloy, *J. Alloys Compd.*, 2016, **661**, p 237–244

11. X. Wu, W. Qin, Y. Guo, and Zh. Xie, Self-Lubricative Coating Grown by Micro-plasma Oxidation on Aluminum Alloys in the Solution of Aluminate–Graphite, *Appl. Surf. Sci.*, 2008, **254**, p 6395–6399

12. L. Rama rishna, A. Sudha Purnima, and G. Sundararajan, A Comparative Study of Tribological Behavior of Micro Arc Oxidation and Hard-Anodized Coatings, *Wear*, 2006, **261**, p 1095–1101

13. S. Moon and Y. Jevon, Generation Mechanism of Micro Discharges During Plasma Electrolytic Oxidation of Al in Aqueous Solutions, *Corros. Sci.*, 2009, **51**, p 1506–1512

14. V. Dehnavi, D.W. Shoesmith, B.L. Luan, M. Yari, X.Y. Liu, and S. Rohani, Corrosion Properties of Plasma Electrolytic Oxidation Coatings on an Aluminum Alloy—The Effect of the PEO Process Stage, *Mater. Chem. Phys.*, 2015, **161**, p 49–58

15. M.M.S. Al Bostaa and K.J. Mab, Suggested Mechanism for the MAO Ceramic Coating on Aluminum Substrates Using Bipolar Current Mode in the Alkaline Silicate Electrolyte, *Appl. Surf. Sci.*, 2014, **308**, p 121–138

16. W.Ch Gu, G.H. Lv, H. Chen, G.L. Chen, W.R. Feng, G.L. Zhang, and S.Z. Yang, Investigation of Morphology and Composition of Plasma Electrolytic Oxidation Coatings in Systems of Na$_2$SiO$_3$-NaOH and (NaPO$_3$)$_6$-NaOH, *Mater. Process. Technol.*, 2007, **182**, p 28–33

17. Ch.Ch. Tseng, J.L. Lee, T.H. Kuo, ShN Kuo, and K.H. Tseng, The Influence of Sodium Tungstate Concentration and Anodizing Conditions on Micro Arc Oxidation (MAO) Coatings for Aluminum Alloy, *Surf. Coat. Technol.*, 2012, **206**, p 3437–3443

18. Zh. Wang, L. Wu, W. Cai, A. Shan, and Zh. Jiang, Effects of Fluoride on the Structure and Properties of Micro Arc Oxidation Coating on Aluminum Alloy, *J. Alloys Compd.*, 2010, **505**, p 188–193

19. R.F. Zhang, Film Formation in the Second Step of Micro-arc Oxidation on Magnesium Alloys, *Corros. Sci.*, 2010, **52**, p 1285–1290

20. M. Tang, W. Li, H. Liu, and L. Zhu, Influence of K$_2$TiF$_6$ in Electrolyte on Characteristics of the Micro Arc Oxidation Coating on Aluminum Alloy, *Curr. Appl. Phys.*, 2012, **12**, p 1259–1265

21. H. Dong, *Surface Engineering of Light Alloys*, Woodhead Publishing Limited, Oxford, 2010

22. M. Tang, W. Li, H. Liu, and L. Zhu, Influence of Titania Sol in the Electrolyte on Characteristics of the Micro Arc Oxidation Coating Formed on 2A70 Aluminum Alloy, *Surf. Coat. Technol.*, 2011, **205**, p 4135–4140

23. K. Venkateswarlu, N. Rameshbabu, D. Sreekanth, M. Sandhyarani, A.C. Bose, V. Muthupandi, and S. Subramanian, Role of Electrolyte Chemistry on Electronic and In Vitro Electrochemical Properties of Micro-arc Oxidized Titanium Films on Cp Ti, *Electrochim. Acta*, 2013, **105**, p 468–480

24. K. Venkateswarlu, N. Rameshbabu, D. Sreekanth, A.C. Bose, V. Muthupandi, N.K. Babu, and S. Subramanian, Role of Electrolyte Additives on In-Vitro Electrochemical Behavior of Micro Arc Oxidized Titania Films on Cp Ti, *Appl. Surf. Sci.*, 2012, **258**, p 6853–6863

25. M. Kaseem, M.P. Kamil, J.H. Kwon, and Y.G. Ko, Effect of Sodium Benzoate on Corrosion Behavior of 6061 Al Alloy Processed by Plasma Electrolytic Oxidation, *Surf. Coat. Technol.*, 2015, **283**, p 268–273

26. F. Liu, J.L. Xu, D.Z. Yu, F.P. Wang, and L.C. Zhao, Effects of Cathodic Voltages on the Structure and Properties of Ceramic Coatings Formed on NiTi Alloy by Micro-arc Oxidation, *Mater. Chem. Phys.*, 2010, **121**, p 172–177

27. M. Shokouhfar, C. Dehghanian, M. Montazeri, and A. Baradaran, Preparation of Ceramic Coating on Ti Substrate by Plasma Electrolytic Oxidation in Different Electrolytes and Evaluation of Its Corrosion Resistance: Part II, *Appl. Surf. Sci.*, 2012, **258**, p 2416–2423

28. A. Fattah-alhosseini and M. Sabaghi Joni, Effect of KOH Concentration on the Microstructure and Electrochemical Properties of MAO-Coated Mg Alloy AZ31B, *J. Mater. Eng. Perform.*, 2015, **24**(9), p 3444–3452

29. A. Fattah-Alhosseini, M. Vakili-Azghandi, and M.K. Keshavarz, Influence of Concentrations of KOH and Na$_2$SiO$_3$ Electrolytes on the Electrochemical Behavior of Ceramic Coatings on 6061 Al Alloy Processed by Plasma Electrolytic Oxidation, *Acta Metall. Sin. (Engl. Lett.)*, 2016, **29**, p 274–281

30. Y.L. Cheng, M.K. Mao, J.H. Cao, and Zh.M. Peng, Plasma Electrolytic Oxidation of an Al-Cu-Li Alloy in Alkaline Aluminate Electrolytes: A Competition Between Growth and Dissolution for the Initial Ultra-Thin Films, *Electrochim. Acta*, 2014, **138**, p 417–429

31. G.L. Song and Z.M. Shi, Corrosion Mechanism and Evaluation of Anodized Magnesium Alloys, *Corros. Sci.*, 2014, **85**, p 126–140

32. Zh. Yao, Zh. Jiang, Sh Xin, X. Sun, and X. Wu, Electrochemical Impedance Spectroscopy of Ceramic Coatings on Ti-6Al-4V by Micro-plasma Oxidation, *Electrochim. Acta*, 2005, **50**, p 3273–3279

33. J. Ma, C.Z. Wang, C.L. Ban, C.Z. Chen, and H.M. Zhang, Pulsed Laser Deposition of Magnesium-Containing Bioactive Glass Film on Porous Tie6Ale4V Substrate Pretreated by Micro-arc Oxidation, *Vacuum*, 2016, **125**, p 48–55

34. D.R. Annett, C. Scourer, G. Irmer, and E. Muller, Electrochemical Corrosion Behaviour of Uncoated and DLC Coated Medical Grade Co28Cr6Mo, *Surf. Coat. Technol.*, 2004, **177–178**, p 830–837

35. Y. Yang and L. Zhou, Improving Corrosion Resistance of Friction Stir Welding Joint of 7075 Aluminum Alloy by Micro-arc Oxidation, *J. Mater. Sci. Technol.*, 2014, **30**(12), p 1251–1254

36. Zh. Lin, H. Yu, S. He, D. Wang, and Ch. Chen, Effect of Na_2WO_4 on Growth Process and Corrosion Resistance of Micro-arc Oxidation Coatings on 2A12 Aluminum Alloys in CH3COONa Electrolyte, *J. Mater. Eng. Perform.*, 2016, **25**, p 297–303

37. B. Rajasekaran, S. Ganesh Sundara Raman, S.V. Joshi, and G. Sundararajan, Effect of Microarc Oxidised Layer Thickness on Plain Fatigue and Fretting Fatigue Behaviour of Al-Mg-Si Alloy, *Int. J. Fatigue*, 2008, **30**, p 1259–1266

38. R.O. Hussein, X. Nie, and D.O. Northwood, A Spectroscopic and Microstructural Study of Oxide Coatings Produced on a Ti-6Al-4V Alloy by Plasma Electrolytic Oxidation, *Mater. Chem. Phys.*, 2012, **134**, p 484–492

39. A.L. Yerokhin, X. Nie, A. Leyland, A. Matthews, and S.J. Dowey, Plasma Electrolysis for Surface Engineering, *Surf. Coat. Technol.*, 1999, **122**, p 73–93

40. L. Rama Krishna, P.S.V.N.B. Gupta, and G. Sundararajan, The Influence of Phase Gradient Within the Micro Arc Oxidation (MAO) Coatings on Mechanical and Tribological Behaviors, *Surf. Coat. Technol.*, 2015, **269**, p 54–63

41. Sh Xin, L. Song, R. Zhao, and X. Hu, Influence of Cathodic Current on Composition, Structure and Properties of Al_2O_3 Coatings on Aluminum Alloy Prepared by Micro-arc Oxidation Process, *Thin Solid Films*, 2006, **515**, p 326–332

42. G. Lv, W. Gu, H. Chen, W. Feng, M.L. Khosa, L. Li, E. Niu, G. Zhang, and S.Z. Yang, Characteristic of Ceramic Coatings on Aluminum by Plasma Electrolytic Oxidation in Silicate and Phosphate Electrolyte, *Appl. Surf. Sci.*, 2006, **253**, p 2947–2952

43. Ch. J. Liang, *In-Situ Impedance Spectroscopy Studies of the Plasma Electrolytic Oxidation Coating Process*, The University of Sheffield, PhD thesis, University of Sheffield, 2013

44. L. Hong-xia, S. Ren-guo, and J. Zhen-guo, Effects of Nano-additive TiO_2 on Performance of Micro-arc Oxidation Coatings Formed on 6063 Aluminum Alloy, *Trans. Nonferrous Met. Soc. China*, 2013, **23**, p 406–411